nature physics
SUPPLEMENTARY INFORMATION
DOI: 10.1038/NPHYS3900

Superfluid Brillouin optomechanics

A.D. Kashkanova,[1] A.B. Shkarin,[1] C. D. Brown,[1] N. E. Flowers-Jacobs,[1] L. Childress,[1,3] S.W. Hoch,[1] L. Hohmann,[3] K. Ott,[3] J. Reichel,[3] and J. G. E. Harris[1,4]

[1]Department of Physics, Yale University, New Haven, CT, 06511, USA
[2]Department of Physics, McGill University, 3600 Rue University, Montreal, Quebec H3A 2T8, Canada
[3]Laboratoire Kastler Brossel, ENS/UPMC-Paris 6/CNRS, F-75005 Paris, France
[4]Department of Applied Physics, Yale University, New Haven, CT, 06511, USA

SI A OMIT/OMIA measurements

SI A.1 Theory

In this section we describe the theory of Optomechanically Induced Transparency and Optomechanically Induced Amplification (OMIT/OMIA) measurements when a slow photothermal process exists in addition to the usual optomechanical coupling. Using the same notation as the main paper, the standard optomechanics Hamiltonian is

$$\hat{\mathcal{H}} = \hbar\omega_\alpha \hat{a}_\alpha^\dagger \hat{a}_\alpha + \hbar\omega_\beta \hat{b}_\beta^\dagger \hat{b}_\beta + \hbar g_0^{\alpha,\beta}(\hat{b}_\beta + \hat{b}_\beta^\dagger)\hat{a}_\alpha^\dagger \hat{a}_\alpha + \hbar\sqrt{\kappa_{\alpha,\mathrm{in}}}(s_{\mathrm{in}}^* \hat{a}_\alpha + s_{\mathrm{in}} \hat{a}_\alpha^\dagger) \tag{1}$$

where $\kappa_{\alpha,in}$ is the input coupling and s_{in} is the amplitude of the incoming laser beam

$$s_{\mathrm{in}} = (\bar{s}_{\mathrm{in}} + \delta s_{\mathrm{in}}(t))e^{-i\omega_{\mathrm{L}} t} \tag{2}$$

Here $\bar{s}_{\mathrm{in}}$ is a strong "control" beam and $\delta s_{\mathrm{in}}(t)$ is a weak "probe" beam.

The Heisenberg equations of motion are

$$\dot{\hat{a}}_\alpha = -i(\omega_\alpha \hat{a}_\alpha + g_0^{\alpha,\beta}(\hat{b}_\beta + \hat{b}_\beta^\dagger)\hat{a}_\alpha + \sqrt{\kappa_{\alpha,\mathrm{in}}} s_{\mathrm{in}}) - \frac{\kappa_\alpha}{2}\hat{a}_\alpha \tag{3}$$

and:

$$\dot{\hat{b}}_\beta = -i(\omega_\beta \hat{b}_\beta + g_0^{\alpha,\beta}\hat{a}_\alpha^\dagger \hat{a}_\alpha) - \frac{\gamma_\beta}{2}\hat{b}_\beta - i g_{\mathrm{T}}\delta T \tag{4}$$

with the damping rates κ_α and γ_β for the cavity field and the acoustic mode correspondingly. Since OMIT/OMIA is a coherent measurement, the thermal noise of the acoustic mode (which is incoherent) can be neglected. The last term in equation 4 describes the driving of the acoustic mode by changes in the helium temperature δT. The acoustic mode is coupled to the temperature fluctuations with the coupling rate g_T which has units of Hz/K. Furthermore, we assume that δT undergoes simple relaxation towards an equilibrium value set by the intracavity photon number.

$$\dot{\delta T} = g_{\mathrm{ta}}\hat{a}_\alpha^\dagger \hat{a}_\alpha - \kappa_{\mathrm{th}}\delta T \tag{5}$$

 DOI: 10.1038/NPHYS3900

In this equation $g_{\rm ta}$ is the single photon heating rate in units of K/s, and κ_{th} is the relaxation rate of the temperature of the helium inside the cavity.

The two beams produce intensity beating with frequency $\Omega_{\rm D} \approx \omega_\beta$ and with amplitude A, so

$$\hat{a}_\alpha^\dagger \hat{a}_\alpha = \bar{n}_\alpha + (Ae^{-i\Omega_{\rm D}t} + \text{c.c.}) \tag{6}$$

Here $\bar{n}_\alpha$ is the average circulating photon number. We combine equation 6 with equation 5 and solve for δT, ignoring the constant temperature shift (due to $\bar{n}_\alpha$). The solution is

$$\delta T = \frac{g_{\rm ta}}{\kappa_{\rm th}} \left(\frac{Ae^{-i\Omega_{\rm D}t}}{1 - i\Omega_{\rm D}/\kappa_{\rm th}} + \text{c.c.} \right) \tag{7}$$

Plugging this back into equation 4 and ignoring the counter-rotating term proportional to $e^{+i\Omega_D t}$ gives

$$\dot{\hat{b}}_\beta = -i \left(\omega_\beta \hat{b}_\beta + g_0^{\alpha,\beta} \bar{n}_\alpha + \left(g_0^{\alpha,\beta} + g_T \frac{g_{\rm ta}}{\kappa_{\rm th}} \frac{1}{1 - i\Omega_{\rm D}/\kappa_{\rm th}} \right) Ae^{-i\Omega_D t} \right) - \frac{\gamma_\beta}{2} \hat{b}_\beta \tag{8}$$

We now define

$$g_{0,\rm pt}^{\alpha,\beta} = g_{\rm T} \frac{g_{\rm ta}}{\kappa_{\rm th}} \frac{1}{i + \Omega_{\rm D}/\kappa_{\rm th}} \approx g_{\rm T} \frac{g_{\rm ta}}{\Omega_{\rm D}} \approx g_{\rm T} \frac{g_{\rm ta}}{\omega_\beta}, \tag{9}$$

where we've assumed that the thermal relaxation rate $\kappa_{\rm th}$ is much smaller than the drive frequency Ω_D. The total coupling to the beat note part of the intracavity power is $g_{\rm tot} = g_0^{\alpha,\beta}(1 + i g_{0,\rm pt}^{\alpha,\beta}/g_0^{\alpha,\beta}) = g_0^{\alpha,\beta} G$, where G is defined as

$$G = 1 + i \frac{g_{0,\rm pt}^{\alpha,\beta}}{g_0^{\alpha,\beta}} \tag{10}$$

With this modification, equation 4 becomes

$$\dot{\hat{b}}_\beta = -i(\omega_\beta \hat{b}_\beta + g_0^{\alpha,\beta} \bar{n}_\alpha + g_0^{\alpha,\beta} G A e^{-i\Omega_D t}) - \frac{\gamma_\beta}{2} \hat{b}_\beta \tag{11}$$

Note that the equation of motion for $\hat{a}_\alpha$ (equation 3) is not influenced by the inclusion of this photothermal process, because the action of the acoustic mode on the intracavity light is only via changes in the He density, which are fully parameterized by $\hat{b}_\beta$.

In the frame rotating at $\omega_{\rm L}$, defining $\Delta = \omega_{\rm L} - \omega_\alpha$, and redefining $\hat{a}_\alpha$ and $s_{\rm in}$ to be rotating at $\omega_{\rm L}$ as well, we have

$$\dot{\hat{a}}_\alpha = i\Delta \hat{a}_\alpha - i g_0^{\alpha,\beta} (\hat{b}_\beta + \hat{b}_\beta^\dagger) \hat{a}_\alpha - i\sqrt{\kappa_{\alpha,\rm in}} s_{\rm in} - \frac{\kappa_\alpha}{2} \hat{a}_\alpha \tag{12}$$

The steady state equations are

$$\bar{a}_\alpha = \frac{-i\sqrt{\kappa_{\alpha,\rm in}} \bar{s}_{\rm in}}{-i\bar{\Delta} + \frac{\kappa_\alpha}{2}} \tag{13}$$

and

$$\bar{b}_\beta = \frac{-i g_0^{\alpha,\beta} |\bar{a}_\alpha|^2}{i\omega_\beta + \frac{\gamma_\beta}{2}} \tag{14}$$

where an effective detuning is defined: $\bar{\Delta} = \Delta - g_0^{\alpha,\beta}(\bar{b}_\beta + \bar{b}_\beta^*)$.

Now we linearize the equations around the mean optical amplitude $\bar{a}$, mean acoustic amplitude $\bar{b}$ and average laser drive $\bar{s}_{in}$, by assuming $\hat{a}_\alpha(t) = \bar{a}_\alpha + \delta\hat{a}_\alpha(t)$, $\hat{b}_\beta(t) = \bar{b}_\beta + \delta\hat{b}_\beta(t)$ and $s_{\text{in}} = \bar{s}_{\text{in}} + \delta s_{\text{in}}(t)$. Plugging this assumption into equations 12 and 4 and making use of equations 13 and 14 we have

$$\delta\dot{\hat{a}}_\alpha(t) = i\bar{\Delta}\delta\hat{a}_\alpha(t) - ig_0^{\alpha,\beta}(\delta\hat{b}_\beta(t) + \delta\hat{b}_\beta^\dagger(t))\bar{a}_\alpha - i\sqrt{\kappa_{\alpha,\text{in}}}\delta s_{\text{in}}(t) - \frac{\kappa_\alpha}{2}\delta\hat{a}_\alpha(t) \tag{15}$$

$$\delta\dot{\hat{b}}_\beta(t) = -i\omega_\beta\delta\hat{b}_\beta(t) - ig_0^{\alpha,\beta}G(\bar{a}^*\delta\hat{a}_\alpha(t) + \bar{a}\delta\hat{a}_\alpha^\dagger(t)) - \frac{\gamma_\beta}{2}\delta\hat{b}_\beta \tag{16}$$

In the equation 16 we recognized that $\bar{a}^*\delta\hat{a}_\alpha(t) + \bar{a}\delta\hat{a}_\alpha^\dagger(t)$ is the term corresponding to the intracavity power beat note that we've denoted as $(Ae^{-i\Omega_D t} + \text{c.c.})$ earlier, so its optomechanical coupling should have the photothermal correction factor G. The Fourier transform of equation 15 is

$$-i\omega\delta\hat{a}_\alpha[\omega] = i\bar{\Delta}\delta\hat{a}_\alpha[\omega] - ig_0^{\alpha,\beta}(\delta\hat{b}_\beta[\omega] + \delta\hat{b}_\beta^\dagger[\omega])\bar{a}_\alpha - i\sqrt{\kappa_{\alpha,\text{in}}}\delta s_{\text{in}}[\omega] - \frac{\kappa_\alpha}{2}\delta\hat{a}_\alpha[\omega] \tag{17}$$

By defining the cavity susceptibility

$$\chi_{\text{cav}}[\omega] = \frac{1}{-i\omega - i\bar{\Delta} + \frac{\kappa_\alpha}{2}} \tag{18}$$

and multiphoton coupling

$$g = g_0^{\alpha,\beta}\bar{a}_\alpha \tag{19}$$

we can rewrite equation 17 and its complex conjugate as

$$\delta\hat{a}_\alpha[\omega] = -i\chi_{\text{cav}}[\omega]\left(g(\delta\hat{b}_\beta[\omega] + \delta\hat{b}_\beta^\dagger[\omega]) + \sqrt{\kappa_{\alpha,\text{in}}}\delta s_{\text{in}}[\omega]\right) \tag{20}$$

$$\delta\hat{a}_\alpha^\dagger[\omega] = i\chi_{\text{cav}}^*[-\omega]\left(g^*(\delta\hat{b}_\beta[\omega] + \delta\hat{b}_\beta^\dagger[\omega]) + \sqrt{\kappa_{\alpha,\text{in}}}\delta s_{\text{in}}^*[\omega]\right) \tag{21}$$

Now we take the Fourier transform of equation 16

$$-i\omega\delta\hat{b}_\beta[\omega] = -i\omega_\beta\delta\hat{b}_\beta[\omega] - iG(g^*\delta\hat{a}_\alpha[\omega] + g\delta\hat{a}_\alpha^\dagger[\omega]) - \frac{\gamma_\beta}{2}\delta\hat{b}_\beta[\omega] \tag{22}$$

Combining equations 20 and 21

$$\begin{aligned}(g^*\delta\hat{a}_\alpha[\omega] + g\delta\hat{a}_\alpha^\dagger[\omega]) =& i|g|^2(\delta\hat{b}_\beta[\omega] + \delta\hat{b}_\beta^\dagger[\omega])(\chi_{\text{cav}}^*[-\omega] - \chi_{\text{cav}}[\omega]) \\ &+ i\sqrt{\kappa_{\alpha,\text{in}}}(\chi_{\text{cav}}^*[-\omega]\delta s_{\text{in}}^*[\omega]g - \chi_{\text{cav}}[\omega]\delta s_{\text{in}}[\omega]g^*)\end{aligned} \tag{23}$$

Since $\gamma_\beta \ll \omega_\beta$, we can neglect the counter-rotating term $\delta\hat{b}_\beta^\dagger[\omega]$, which is peaked around $-\omega_\beta$, so

$$\delta\hat{b}_\beta[\omega] = \frac{G\sqrt{\kappa_{\alpha,\text{in}}}(\chi_{\text{cav}}^*[-\omega]\delta s_{\text{in}}^*[\omega]g - \chi_{\text{cav}}[\omega]\delta s_{\text{in}}[\omega]g^*)}{-i(\omega - \omega_\beta) + \frac{\gamma_\beta}{2} + G|g|^2(\chi_{\text{cav}}[\omega] - \chi_{\text{cav}}^*[-\omega])} \tag{24}$$

Defining

$$i\Sigma[\omega] = G|g|^2(\chi_{\text{cav}}[\omega] - \chi_{\text{cav}}^*[-\omega]) \tag{25}$$

 DOI: 10.1038/NPHYS3900

results in

$$\delta\hat{b}_\beta[\omega] = \frac{G\sqrt{\kappa_{\alpha,\mathrm{in}}}(\chi^*_{\mathrm{cav}}[-\omega]\delta s^*_{\mathrm{in}}[\omega]g - \chi_{\mathrm{cav}}[\omega]\delta s_{\mathrm{in}}[\omega]g^*)}{-i(\omega-\omega_\beta)+\frac{\gamma_\beta}{2}+i\Sigma[\omega]} \tag{26}$$

In this notation the optical spring $\Delta\omega_{\beta(\mathrm{opt})}$ and optical damping $\gamma_{\beta(\mathrm{opt})}$ are correspondingly

$$\Delta\omega_{\beta(\mathrm{opt})} = \mathrm{Re}[\Sigma[\omega]] \tag{27}$$

$$\gamma_{\beta(\mathrm{opt})} = -2\mathrm{Im}[\Sigma[\omega]] \tag{28}$$

Now we calculate the amplitude and phase of the OMIA signal. In order to observe OMIT/OMIA it is necessary to have two beams detuned by a frequency nearly equal to that of the acoustic oscillator. As shown by equation 2, there are two beams in the system: a strong control beam and a weak probe beam. The probe beam is detuned from the control beam by $-\Omega$, where $\Omega > 0$. In the rotating frame, the expression for $\delta s_{\mathrm{in}}(t)$ is

$$\delta s_{\mathrm{in}}(t) = s_{\mathrm{p}}e^{i\Omega t} \tag{29}$$

Taking the Fourier transform and assuming s_p to be real

$$\delta s_{\mathrm{in}}[\omega] = \sqrt{2\pi}s_{\mathrm{p}}\delta(\omega+\Omega) \tag{30}$$

Putting this back into equation 24

$$\delta\hat{b}_\beta[\omega] = \frac{\sqrt{2\pi}s_{\mathrm{p}}G\sqrt{\kappa_{\alpha,\mathrm{in}}}(g\chi^*_{\mathrm{cav}}[-\omega]\delta(\omega-\Omega) - g^*\chi_{\mathrm{cav}}[\omega]\delta(\omega+\Omega))}{-i(\omega-\omega_\beta)+\frac{\gamma_\beta}{2}+i\Sigma[\omega]} \tag{31}$$

Going back into the time domain

$$\delta\hat{b}_\beta(t) = b_+[\Omega]s_{\mathrm{p}}e^{-i\Omega t} + b_-[\Omega]s_{\mathrm{p}}e^{i\Omega t} \tag{32}$$

where

$$b_+[\Omega] = \frac{G\sqrt{\kappa_{\alpha,\mathrm{in}}}\chi^*_{\mathrm{cav}}[-\Omega]g}{-i(\Omega-\omega_\beta)+\frac{\gamma_\beta}{2}+i\Sigma[\Omega]} \tag{33}$$

and

$$b_-[\Omega] = \frac{G\sqrt{\kappa_{\alpha,\mathrm{in}}}(-\chi_{\mathrm{cav}}[-\Omega]g^*)}{-i(-\Omega-\omega_\beta)+\frac{\gamma_\beta}{2}+i\Sigma[-\Omega]} \tag{34}$$

The expression for b_+ gives the complex amplitude of the acoustic oscillator. Oscillating at $-\Omega$, b_- is far off resonance, so it will be small.

The optical amplitude is given by equation 20 as

$$\delta\hat{a}_\alpha[\omega] = -i\chi_{\mathrm{cav}}[\omega]\left(g(\delta\hat{b}_\beta[\omega]+\delta\hat{b}^\dagger_\beta[\omega]) + \sqrt{\kappa_{\alpha,\mathrm{in}}}\delta s_{\mathrm{in}}[\omega]\right) \tag{35}$$

Recasting the acoustic mode amplitude in the time domain and neglecting b_- yields

$$g(\delta\hat{b}_\beta(t)+\delta\hat{b}^\dagger_\beta(t)) + \sqrt{\kappa_{\alpha,\mathrm{in}}}\delta s_{\mathrm{in}}(t) = \left(gb_+[\Omega]e^{-i\Omega t} + \left(gb^*_+[\Omega]+\sqrt{\kappa_{\alpha,\mathrm{in}}}\right)e^{i\Omega t}\right)s_{\mathrm{p}} \tag{36}$$

We express the cavity mode amplitude as

$$\delta\hat{a}_\alpha(t) = a_+[\Omega]e^{-i\Omega t} + a_-[\Omega]e^{i\Omega t} \tag{37}$$

where

$$a_+[\Omega] = -i\chi_{\text{cav}}[\Omega] g b_+[\Omega] s_{\text{p}} \tag{38}$$

and

$$a_-[\Omega] = -i\chi_{\text{cav}}[-\Omega] \left(g b_+^*[\Omega] + \sqrt{\kappa_{\alpha,\text{in}}}\right) s_{\text{p}} \tag{39}$$

In the measurement scheme employed in the experiment (having a probe beam only at $-\Omega$) only a_- can be measured. In figure 2 of the main paper, we plot a_- normalized with respect to the background. This normalized signal a'_- is given by:

$$a'_-[\Omega] = \frac{a_-[\Omega]}{a_-[\infty]} = \frac{g b_+^*[\Omega]}{\sqrt{\kappa_{\alpha,\text{in}}}} + 1 \tag{40}$$

The functions $a[\Omega]$ and $\psi[\Omega]$ are the magnitude and phase of $a'_-[\Omega]$. The values A and Ψ, described in the main paper are found as follows

$$A = \text{abs}\left[\frac{g b_+^*[\omega_\beta]}{\sqrt{\kappa_{\alpha,\text{in}}}}\right] \tag{41}$$

$$\Psi = \arg\left[\frac{g b_+^*[\omega_\beta]}{\sqrt{\kappa_{\alpha,\text{in}}}}\right] \tag{42}$$

Where $b_+^*[-\omega_\beta]$ is the complex amplitude of the acoustic oscillator, when the the probe beam is detuned by $-\omega_\beta$ from the control beam.

SI A.2 Full treatment of phase modulation.

In order to use the treatment above to describe the measurements discussed in the main text, we need to take into account some additional features of the measurement setup.

First, as mentioned in the main text, the probe and the control beams are generated in a phase modulator. Specifically, two microwave tones drive the phase modulator: a stronger one at frequency ω_{control}, and a weaker one at $\omega_{\text{probe}} = \omega_{\text{control}} + \Omega$ (in the actual experiment we also send a third, even weaker, tone that is used for locking the laser to the cavity; its power is at least 3 times lower than the probe tone and it is at a different frequency, so it has a negligible effect on the measurement result). The strong and the weak microwave tones generate the control and the probe optical tones respectively, while the optical carrier acts as a local oscillator in the heterodyne measurement. However, phase modulation generates sidebands symmetrically about the carrier, resulting in negative-order sidebands on the other side of the carrier. These are far enough detuned from the cavity that they don't noticeably affect the mechanical motion; nevertheless, their beat notes with the carrier are phase-coherent with the beat notes produced by the control and probe beams, so they will partially cancel the expected heterodyne signal, thus influencing the measurement result.

Moreover, in some of the measurements the microwave tones are strong enough that we need to take into account higher-order optical sidebands (e.g., at frequencies $2\omega_{\text{control}}$ or $\omega_{\text{control}} + \omega_{\text{probe}}$). These can contribute to the beat note in the photocurrent, and can also be close enough to the cavity resonance to influence mechanical motion.

Finally, the local oscillator is not infinitely far detuned from the cavity (in our case, it is detuned by $\sim 15\kappa$). Hence, it experiences some cavity-induced phase shift in reflection, which also needs to be taken into account.

DOI: 10.1038/NPHYS3900

In order to consistently account for all the factors listed above, we start with the description of the phase modulator. We denote the incident optical tone by $a_0 e^{-i\omega_0 t}$, and a set of microwave tones by $\phi_n \cos(\omega_n t)$, where the ϕ_n are the microwave amplitudes normalized by the (possibly frequency-dependent) V_π of the phase modulator, and the ω_n are the corresponding microwave frequencies. The output of the modulator is then expressed as

$$a_\phi = a_0 e^{-i\omega_0 t} e^{i\sum_n \phi_n \cos(\omega_n t)} = a_0 e^{-i\omega_0 t} \prod_n e^{i\phi_n \cos(\omega_n t)} \tag{43}$$

Next, we use the Jacobi-Anger expansion for the exponents

$$e^{i\phi_n \cos(\omega_n t)} = \sum_{k=-\infty}^{+\infty} (-i)^k J_k(\phi_n) e^{-ik\omega_n t}, \tag{44}$$

where $J_k(z)$ is k^{th} Bessel function of the first kind. With this, the output laser becomes

$$a_\phi = a_0 e^{-i\omega_0 t} \prod_n \left[\sum_{k=-\infty}^{+\infty} (-i)^k J_k(\phi_n) e^{-ik\omega_n t} \right] \equiv e^{-i\omega_0 t} \sum_l a_l e^{-i\omega_l t}, \tag{45}$$

where ω_l are all possible intermodulation frequencies resulting from the ω_n. In practice, to keep the computation time short we limit our calculations to a finite intermodulation order (as discussed below).

Next, we consider all of these beams (including the carrier) landing on the cavity. To recap equations 12 and 11, the equations of motion can be written as

$$\dot{a}_\alpha = -(\kappa_\alpha/2 + i\omega_\alpha)a_\alpha - ig_0^{\alpha,\beta} a_\alpha (b_\beta + b_\beta^*) - i\sqrt{\kappa_{\alpha,\text{in}}} s_{\text{in}} \tag{46}$$

$$\dot{b}_\beta = -(\gamma_\beta/2 + i\omega_\beta)b_\beta - ig_0^{\alpha,\beta} G a_\alpha^* a_\alpha \tag{47}$$

In the frame rotating at the carrier frequency ω_0 the incident optical field becomes $s_{\text{in}} = \sum_l a_l e^{-i\omega_l t}$, and the optical equation of motion can be written as

$$\dot{a}_\alpha = -(\kappa_\alpha/2 - i\Delta)a_\alpha - ig_0^{\alpha,\beta} a_\alpha (b_\beta + b_\beta^*) - i\sqrt{\kappa_{\alpha,\text{in}}} \sum_l a_l e^{-i\omega_l t}, \tag{48}$$

with $\Delta = \omega_0 - \omega_\alpha$ being the carrier (i.e., local oscillator) detuning.

As usual, next we linearize this equation. To zeroth order in $g_0^{\alpha,\beta}$, the field amplitude is

$$a_0 = \sum_l a_{l,0} e^{-i\omega_l t} \tag{49}$$

$$a_{l,0} = -i\sqrt{\kappa_{\alpha,\text{in}}} a_l \chi_{\text{cav}}[\omega_l], \tag{50}$$

where $\chi_{\text{cav}}[\omega] = (\kappa_\alpha/2 - i(\omega + \Delta))^{-1}$. This amplitude results in a force on the mechanical oscillator given by

$$F_0 = -ig_0^{\alpha,\beta} G a_0^* a_0 = -ig_0^{\alpha,\beta} G \sum_l \sum_k a_{l,0} a_{k,0}^* e^{-i(\omega_l - \omega_k)t} \tag{51}$$

The first order in $g_0^{\alpha,\beta}$ terms due to the mechanical motion are (in the adiabatic regime, where $\gamma_\beta \ll \kappa_\alpha$)

$$a_1 = -ig_0^{\alpha,\beta} \sum_l a_{l,0} e^{-i\omega_l t} \left(b_\beta \chi_{\text{cav}}[\omega_l + \omega_\beta] + b_\beta^* \chi_{\text{cav}}[\omega_l - \omega_\beta] \right) \tag{52}$$

Their contribution to the mechanical force is

$$\begin{aligned} F_1 &= -ig_0^{\alpha,\beta} G (a_0^* a_1 + a_0 a_1^*) \\ &= (g_0^{\alpha,\beta})^2 G \sum_l \sum_k a_{l,0} a_{k,0}^* e^{-i(\omega_l - \omega_k)t} \left[b_\beta \left(\chi_{\text{cav}}^*[\omega_k - \omega_\beta] - \chi_{\text{cav}}[\omega_l + \omega_\beta] \right) \right. \\ &\qquad \left. + b_\beta^* \left(\chi_{\text{cav}}^*[\omega_k + \omega_\beta] - \chi_{\text{cav}}[\omega_l - \omega_\beta] \right) \right] \end{aligned} \tag{53}$$

We can make a couple of simplifying assumptions. First, we note that b_β rotates at $+\omega_\beta$, while b_β^* is located around $-\omega_\beta$. This means that they will be coupled only by the terms rotating at $2\omega_\beta$ (i.e., for $|\omega_k - \omega_l| \approx 2\omega_\beta$). In our case, these terms should be very small, since they would only come from the higher (at least, fourth) order in sideband amplitudes. Thus, we can neglect the b_β^* term and get

$$F_1 = -i\Sigma b_\beta \tag{54}$$

$$\Sigma = i(g_0^{\alpha,\beta})^2 G \sum_l \sum_k a_{l,0} a_{k,0}^* e^{-i(\omega_l - \omega_k)t} \left(\chi_{\text{cav}}^*[\omega_k - \omega_\beta] - \chi_{\text{cav}}[\omega_l + \omega_\beta] \right) \tag{55}$$

Second, we are predominantly interested in the DC terms in Σ; everything else will result in terms rotating at frequencies other than ω_β and, again, will end up far away from the acoustic resonance. As a result, the acoustic equation of motion becomes

$$\dot{b}_\beta = -(\gamma_\beta/2 + i\omega_\beta + i\Sigma) b_\beta + F_0 \tag{56}$$

$$\Sigma = i(g_0^{\alpha,\beta})^2 G \sum_l |a_{l,0}|^2 \left(\chi_{\text{cav}}^*[\omega_l - \omega_\beta] - \chi_{\text{cav}}[\omega_l + \omega_\beta] \right) \tag{57}$$

The solution for this equation is

$$b_\beta = -i(g_0^{\alpha,\beta})^2 G \sum_l \sum_k \chi_{\beta,\text{eff}}[\omega_l - \omega_k] a_{l,0} a_{k,0}^* e^{-i(\omega_l - \omega_k)t} \tag{58}$$

$$\chi_{\beta,\text{eff}}[\omega] = (\gamma_\beta/2 + i\omega_\beta + i\Sigma - i\omega)^{-1} \tag{59}$$

Finally, knowing this expression for b_β we can obtain the intracavity power using the first-order solution (equation (52)). Some of the terms in a_1 will end up being phase-coherent with the initial optical drive (e.g., the motional sideband on the control beam will be phase-coherent with the probe beam, and vice versa). It is these terms that will define the OMIT response.

For the analysis presented in the main body of the paper, we implement this procedure as follows

- First, knowing the microwave drives and phase modulator response, calculate the tones on the output of the phase modulator using equation 45 (for practical reasons, we limit expansion to the third order in the control beam amplitude and to the first order in the probe beam amplitude);
- Next, from equations 49 and 50 determine the zeroth order intracavity field;

 DOI: 10.1038/NPHYS3900

- Use this to calculate the optical force (equation 51) and self-energy (equation 57);
- From these, determine the mechanical response (equations 58 and 59);
- Use this calculated response to get the resulting field inside the cavity $a_\alpha = a_0 + a_1$, where a_1 is determined by equation 52
- The reflected field is found using the standard input-output relations $a_{\alpha,\text{out}} = a_{\alpha,\text{in}} - i\sqrt{\kappa_{\alpha,\text{in}}}a_\alpha$;
- Finally, to relate this field to the measurable quantities, we calculate the electrical response of the photodiode $I \propto a^*_{\alpha,\text{out}}a_{\alpha,\text{out}}$, which will consist of all possible beat notes of the reflected optical tones. The amplitude of the electrical tone oscillating at ω_probe (which mainly comes of the beating of the probe beam with the carrier) is the relevant OMIT signal.

All of these calculation are performed numerically.

SI B Optical and acoustic transmission of the cavity mirrors

SI B.1 General considerations

A cavity made of two lossless mirrors with power transmittances T_1 and T_2 has finesse [1]

$$\mathcal{F} = \frac{2\pi}{T_1 + T_2} \tag{60}$$

The corresponding quality factor is

$$Q = \frac{f}{\gamma} = \mathcal{F}\frac{f}{FSR} = \frac{\mathcal{F}f(2L)}{v} = \frac{4\pi f L}{v(T_1 + T_2)} \tag{61}$$

Here f and γ are the frequency and linewidth of the cavity mode, L is the cavity length and v is the speed of wave propagation (either optical or acoustic). A conventional way of creating mirrors with very low loss and low transmission is by using Distributed Bragg Reflectors (DBRs).

SI B.2 The optical transmission through a DBR

This brief review follows the treatment in ref.[2]. Figure 1 shows a schematic representation of a DBR, where the amplitude of the incident field is $E^{(\text{i})} = 1$, the amplitudes of reflected and transmitted fields are $E^{(\text{r})}$ and $E^{(\text{t})}$ correspondingly and the amplitude of the fields propagating forward and backward in the j^th layer are $E_j^{(\text{f})}$ and $E_j^{(\text{b})}$ correspondingly. The index of refraction of the material from which the wave is incident is n_i and the index of refraction of the material into which the wave is transmitted is n_t. The index of refraction of the j^th layer is n_j and the thickness of the j^th layer is d_j. The x-axis is pointing to the right.

Assume a plane wave approaches the DBR at normal incidence. The continuity of parallel components of electric and magnetic fields at each interface results in the following boundary conditions

$$E_j(x,t) = E_{j+1}(x,t) \tag{62}$$

$$\frac{dE_j(x,t)}{dx} = \frac{dE_{j+1}(x,t)}{dx} \tag{63}$$

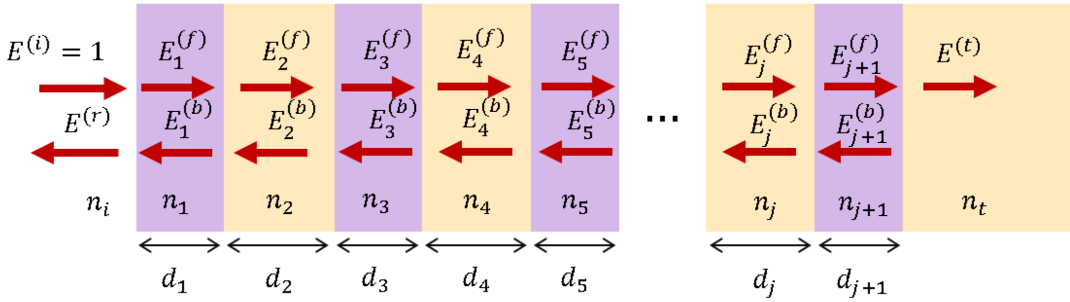

Figure 1: DBR showing the electric field in each layer. Color indicates different materials.

At the first interface, the boundary conditions give

$$1 + E^{(\mathrm{r})} = E_1^{(\mathrm{f})} + E_1^{(\mathrm{b})} \tag{64}$$

$$n_i\left(1 - E^{(\mathrm{r})}\right) = n_1\left(E_1^{(\mathrm{f})} - E_1^{(\mathrm{b})}\right) \tag{65}$$

Applying the boundary conditions to the interface between the j^{th} and $(j+1)^{\mathrm{th}}$ layers yields the equations

$$E_j^{(\mathrm{f})} e^{ikn_jd_j} + E_j^{(\mathrm{b})} e^{-ikn_jd_j} = E_{j+1}^{(\mathrm{f})} + E_{j+1}^{(\mathrm{b})} \tag{66}$$

$$n_j\left(E_j^{(\mathrm{f})} e^{ikn_jd_j} - E_j^{(\mathrm{b})} e^{-ikn_jd_j}\right) = n_{j+1}\left(E_{j+1}^{(\mathrm{f})} - E_{j+1}^{(\mathrm{b})}\right) \tag{67}$$

Assuming the total number of layers is p, applying boundary conditions to the last interface yields

$$E_p^{(\mathrm{f})} e^{ikn_pd_p} + E_p^{(\mathrm{b})} e^{-ikn_pd_p} = E^{(\mathrm{t})} \tag{68}$$

$$n_p\left(E_p^{(\mathrm{f})} e^{ikn_pd_p} - E_p^{(\mathrm{b})} e^{-ikn_pd_p}\right) = n_t E^{(\mathrm{t})} \tag{69}$$

Expressing the equations 64-69 in matrix form

$$\begin{bmatrix} 1 & 1 \\ n_i & -n_i \end{bmatrix} \begin{bmatrix} 1 \\ E^{(\mathrm{r})} \end{bmatrix} = \begin{bmatrix} 1 & 1 \\ n_1 & -n_1 \end{bmatrix} \begin{bmatrix} E_1^{(\mathrm{f})} \\ E_1^{(\mathrm{b})} \end{bmatrix} \tag{70}$$

$$\begin{bmatrix} e^{ikn_jd_j} & e^{-ikn_jd_j} \\ n_je^{ikn_jd_j} & -n_je^{-ikn_jd_j} \end{bmatrix} \begin{bmatrix} E_j^{(\mathrm{f})} \\ E_j^{(\mathrm{b})} \end{bmatrix} = \begin{bmatrix} 1 & 1 \\ n_{j+1} & -n_{j+1} \end{bmatrix} \begin{bmatrix} E_{j+1}^{(\mathrm{f})} \\ E_{j+1}^{(\mathrm{b})} \end{bmatrix} \tag{71}$$

$$\begin{bmatrix} e^{ikn_pd_p} & e^{-ikn_pd_p} \\ n_pe^{ikn_pd_p} & -n_pe^{-ikn_pd_p} \end{bmatrix} \begin{bmatrix} E_p^{(\mathrm{f})} \\ E_p^{(\mathrm{b})} \end{bmatrix} = \begin{bmatrix} 1 & 0 \\ n_t & 0 \end{bmatrix} \begin{bmatrix} E^{(\mathrm{t})} \\ 0 \end{bmatrix} \tag{72}$$

Upon rearranging and combining equations 70-72 we arrive at

$$\begin{bmatrix} 1 \\ E^{(\mathrm{r})} \end{bmatrix} = \begin{bmatrix} 1 & 1 \\ n_i & -n_i \end{bmatrix}^{-1} \prod_{j=1}^{p} M_j \begin{bmatrix} 1 & 0 \\ n_t & 0 \end{bmatrix} \begin{bmatrix} E^{(\mathrm{t})} \\ 0 \end{bmatrix} \tag{73}$$

 DOI: 10.1038/NPHYS3900

where M_j is defined as

$$M_j = \begin{bmatrix} 1 & 1 \\ n_j & -n_j \end{bmatrix} \begin{bmatrix} e^{ikn_jd_j} & e^{-ikn_jd_j} \\ n_je^{ikn_jd_j} & -n_je^{-ikn_jd_j} \end{bmatrix}^{-1} \tag{74}$$

We define:

$$A = \begin{bmatrix} a_{11} & a_{12} \\ a_{21} & a_{22} \end{bmatrix} = \begin{bmatrix} 1 & 1 \\ n_i & -n_i \end{bmatrix}^{-1} \prod_{j=1}^{p} M_j \begin{bmatrix} 1 & 0 \\ n_t & 0 \end{bmatrix} \tag{75}$$

and now we have

$$\begin{bmatrix} 1 \\ E^{(\mathrm{r})} \end{bmatrix} = A \begin{bmatrix} E^{(\mathrm{t})} \\ 0 \end{bmatrix} \tag{76}$$

from which we find

$$r_{\mathrm{opt}} = E^{(\mathrm{r})} = a_{21}/a_{11} \tag{77}$$

$$T_{\mathrm{opt}} = 1 - r_{\mathrm{opt}}^2 \tag{78}$$

To conclude, finding the transmittivity of the DBR involves calculating the matrix A, which is straightforward, provided we know the indexes of refraction n_{i} and n_{t}, and the structure of the DBR, which is fully described by n and d of the alternating DBR layers.

SI B.3 The acoustic transmission through a DBR

Finding the DBR transmittivity for the sound wave is done in a similar manner [3, 4]. Assume a sound wave with frequency f and wavelength λ is incident on a DBR. Equating the displacements $(s(x,t))$ and pressures $(P(x,t) = -K ds/dx)$ on both sides of the boundary (K is the bulk modulus) gives

$$s_j(d,t) = s_{j+1}(d,t) \tag{79}$$

$$K_j \frac{ds_j}{dx}(d,t) = K_{j+1} \frac{ds_{j+1}}{dx}(d,t) \tag{80}$$

The fact that acoustic impedance is related to bulk modulus via $Z = K/v = v\rho$, where ρ is the density of the material, and that the frequency of the mode must be constant throughout the DBR, results in three sets of equations that provide information about the amplitude of the acoustic mode at different interfaces. At the first interface

$$1 + s^{(\mathrm{r})} = s_1^{(\mathrm{f})} + s_1^{(\mathrm{b})} \tag{81}$$

$$Z_i(1 - s^{(\mathrm{r})}) = Z_1 \left(s_1^{(\mathrm{f})} - s_1^{(\mathrm{b})} \right) \tag{82}$$

At the interface between the j^{th} and $(j+1)^{\mathrm{th}}$ layer:

$$s_j^{(\mathrm{f})} e^{ikn_j^{\mathrm{ac}}d_j} + s_j^{(\mathrm{b})} e^{-ikn_j^{\mathrm{ac}}d_j} = s_{j+1}^{(\mathrm{f})} + s_{j+1}^{(\mathrm{b})} \tag{83}$$

$$Z_j \left(s_j^{(\mathrm{f})} e^{ikn_j^{\mathrm{ac}}d_j} - s_j^{(\mathrm{b})} e^{-ikn_j^{\mathrm{ac}}d_j} \right) = Z_{j+1} \left(s_{j+1}^{(\mathrm{f})} - s_{j+1}^{(\mathrm{b})} \right) \tag{84}$$

Here we defined $k = 2\pi/\lambda$ and $n_j^{\mathrm{ac}} = v_i/v_j$, where v_i and v_j are correspondingly the speed of the sound wave in the medium on the incident side and the speed of sound in the j^{th} layer. At the last interface, assuming a total number of layers p

$$s_p^{(\mathrm{f})} e^{ikn_p^{\mathrm{ac}} d_p} + s_p^{(\mathrm{b})} e^{-ikn_p^{\mathrm{ac}} d_p} = s^{(\mathrm{t})} \tag{85}$$

$$Z_p \left(s_p^{(\mathrm{f})} e^{ikn_p^{\mathrm{ac}} d_p} - s_p^{(\mathrm{b})} e^{-ikn_p^{\mathrm{ac}} d_p} \right) = Z_t s^{(\mathrm{t})} \tag{86}$$

From equations 81-86, using the same methods as in section SI B.2 , a matrix B is obtained:

$$B = \begin{bmatrix} b_{11} & b_{12} \\ b_{21} & b_{22} \end{bmatrix} = \begin{bmatrix} 1 & 1 \\ Z_i & -Z_i \end{bmatrix}^{-1} \prod_{j=1}^{p} M_j^{\mathrm{ac}} \begin{bmatrix} 1 & 0 \\ Z_t & 0 \end{bmatrix} \tag{87}$$

where M_j^{ac} is defined as:

$$M_j^{\mathrm{ac}} = \begin{bmatrix} 1 & 1 \\ Z_j & -Z_j \end{bmatrix} \begin{bmatrix} e^{ikn_j^{\mathrm{ac}} d_j} & e^{-ikn_j^{\mathrm{ac}} d_j} \\ Z_j e^{ikn_j^{\mathrm{ac}} d_j} & -Z_j e^{-ikn_j^{\mathrm{ac}} d_j} \end{bmatrix}^{-1} \tag{88}$$

Now we have:

$$\begin{bmatrix} 1 \\ s^{(\mathrm{r})} \end{bmatrix} = B \begin{bmatrix} s^{(\mathrm{t})} \\ 0 \end{bmatrix} \tag{89}$$

from which we get:

$$r_{\mathrm{ac}} = s^{(\mathrm{r})} = b_{21}/b_{11} \tag{90}$$

$$T_{\mathrm{ac}} = 1 - r_{\mathrm{ac}}^2 \tag{91}$$

In conclusion, to calculate both optical and acoustic reflection/transmission of a DBR the following quantities need to be known:

- d -thickness of each layer
- n_{opt} - optical index of refraction for each layer
- ρ - density for each layer
- v - sound velocity in each layer

Additionally, it is necessary to know the values of those parameters for the material from which the wave is incident and the material into which the wave is transmitted. For the experiments described in the main paper these are liquid ^{4}He and SiO_2 respectively.

SI B.4 Optical and acoustic quality factors for the present DBRs

The DBRs in these experiments are deposited on to the faces of SiO_2 fibers. The DBR is comprised of alternating layers of SiO_2 and Ta_2O_5 whose thicknesses are chosen to correspond to one-quarter wavelength of the light (which in vacuum has wavelength $\sim$ 1550 nm). The cavity is formed between two such fibers immersed in superfluid helium; therefore we are interested in the transmission of light and sound from the superfluid helium, through the DBR, and into the fiber.

DOI: 10.1038/NPHYS3900

Material	n_{opt}	v**(m/s)**	ρ **(kg/m^3)**
^{4}He	1.0282[5]	238[5]	145[5]
SiO_2	1.4746[6]	5,900 $\pm$ 100[7, 8]	2,200[7]
Ta_2O_5	2.0483[6]	4,500 $\pm$ 500[7]	7,600 $\pm$ 600[7]

Supplementary Table 1: Material properties of superfluid ^{4}He, SiO_2 and Ta_2O_5

Table 1 shows the relevant parameters for each material.

For the 1550 nm light, a quarter optical wavelength layer of SiO_2 is 263 nm and a quarter optical wavelength layer of Ta_2O_5 is 189 nm. The 1550 nm light has wavelength equal to 1508 nm in liquid ^{4}He and therefore couples to the acoustic mode with 754 nm wavelength in liquid ^{4}He, whose frequency is 315.7 MHz. For this mode, a quarter acoustic wavelength in SiO_2 is 4.7 ± 0.1 μm and a quarter acoustic wavelength in Ta_2O_5 is 3.6 ± 0.4 μm; the large discrepancy between the optical and acoustic wavelengths *in the solid materials* means that the DBRs used in the present device will not provide strong reflectivity for the acoustic waves.

The experiment was performed with the mirror surfaces separated by 84 μm. The cavity consisted of a low reflectivity (15 layer pairs) input DBR and high reflectivity (18 layer pairs) back DBR. The laser wavelength was 1538 nm; the frequency of the acoustic mode of interest was $\omega_\beta = 2\pi \times 317.3$ MHz.

As mentioned above, the DBRs in the present devices are not designed to be highly reflective for the acoustic waves; nevertheless, the strong contrast in acoustic impedance between ^{4}He and the outermost layer of the optical DBR provides fairly large reflectivity. From equation 91 the acoustic transmittivity for the low reflectivity DBR is calculated to be 10,100 $\pm$ 400 ppm, while the acoustic transmittivity for the high reflectivity DBR is calculated to be 7,700 $\pm$ 1,300 ppm. The uncertainties predominantly come from the material properties of Ta_2O_5 (see Table 1). These values of the acoustic transmission lead to the acoustic quality factor $Q_{\beta,\mathrm{ext}}$ =79,000 $\pm$ 5,000 which is slightly higher than the experimentally determined quality factor $Q_{\beta,\mathrm{ext}}$ =70,000 $\pm$ 2,000. This difference might be attributed to various factors, such as losses due to mirror misalignment or imprecise knowledge of the DBR structure.

SI B.5 Improving the acoustic quality factor in future devices

In this section we consider the possibility of improving the acoustic quality factor by adding an acoustic DBR between the substrate and the optical DBR. The proposed structure in shown in figure 2.

We consider a cavity in which optical confinement is again provided by optical DBRs with 15 and 18 pairs, optimized for maximum reflectivity at 1550 nm, and the acoustic confinement is enhanced by additional layers forming an acoustic DBR. Technical aspects of the coating process impose the requirement that the total stack thickness be less than 25 μm, and that the thickness of each layer of a given material is an integer multiple of the thickness of the thinnest layer of this material[6]. Maximizing $Q_{\beta,\mathrm{ext}}$ for the 315.7 MHz acoustic mode (to which 1550 nm light couples), subject to the above constraints, we find the optimal design for the stack. Table 2 shows stack parameters for the current designs as well as the proposed designs.

We use equations 78 and 91 to calculate the optical and acoustic transmission for the DBRs presented in table 2. The results are shown in table 3. The optical transmission doesn't change appreciably as more

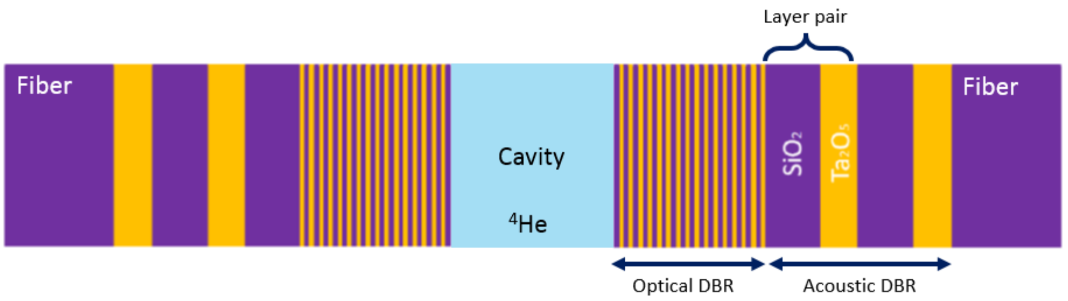

Figure 2: Example of a DBR structure that would be reflective for both optical and acoustic waves

Number	Design
1 (Current)	Substrate$\times$(189 nm $Ta_2O_5$$\times$253 nm SiO_2)^{15}$\times$189 nm Ta_2O_5
2 (Current)	Substrate$\times$(189 nm $Ta_2O_5$$\times$253 nm SiO_2)^{18}$\times$189 nm Ta_2O_5
3 (Future)	Substrate$\times$3591 nm $Ta_2O_5$$\times$4554 nm $SiO_2$$\times$3591 nm $Ta_2O_5$$\times$759 nm $SiO_2$$\times$ (189 nm $Ta_2O_5$$\times$253 nm SiO_2)^{15}$\times$189 nm Ta_2O_5
4 (Future)	Substrate$\times$3780 nm $Ta_2O_5$$\times$4554 nm $SiO_2$$\times$3213 nm $Ta_2O_5$$\times$ (253 nm $SiO_2$$\times$189 nm Ta_2O_5)^{18}

Supplementary Table 2: The stack designs used in the current device and the future stack designs

acoustic layers are added, as the acoustic layers are outside of the optical mode. At the same time, the acoustic layers decrease the acoustic transmission by more than an order of magnitude. Assuming the

Number	T_{opt} (ppm)	T_{ac} (ppm)	d_{total} (μm)	$\frac{U^{\text{SiO}_2}}{U^{\text{He}}}$ (ppm)	$\frac{U^{\text{Ta}_2\text{O}_5}}{U^{\text{He}}}$ (ppm)	$Q_{\beta,\text{loss}}$
1	73.5	$10,000 \pm 400$	6.6	6.5 ± 0.5	17.1 ± 2.1	4.2×10^7
2	10.2	$8,100 \pm 1200$	8.3	6.4 ± 0.9	16.8 ± 1.5	4.3×10^7
3	73.5	350 ± 200	19.68	3.8 ± 1	9.5 ± 2	7.5×10^7
4	10.2	420 ± 240	19.87	3.1 ± 1	7.8 ± 1.4	9.2×10^7

Supplementary Table 3: The calculated parameters for different stacks. The optical transmittivity (T_{opt}), acoustic transmittivity (T_{ac}) and thickness (d_{total}) are discussed in section SI B.5. The ratios of the energy stored in SiO_2 ($U^{\text{SiO}_2}/U^{\text{He}}$) and Ta_2O_5 ($U^{\text{Ta}_2\text{O}_5}/U^{\text{He}}$) to the energy stored in Helium are discussed in SI B.6

mirror separation is 84 μm (as in the present devices), we calculate the expected acoustic quality factor to be $Q_{\beta,\text{ext}} = 3.3 \pm 2.2 \times 10^6$, where the uncertainly is primarily due to the acoustic parameters of Ta_2O_5. This calculation assumes a cavity constructed from Device #3 and Device #4 in Tables 2 and 3.

DOI: 10.1038/NPHYS3900

SI B.6 Acoustic loss inside the DBR layers

In addition to being limited by the transmission of the acoustic mode into the fiber, the acoustic Q factor can also be limited by dissipation in the DBR. To estimate the Q factor associated with this loss, the following expression is used

$$\frac{1}{Q_{\beta,\mathrm{loss}}} = \frac{U^{\mathrm{SiO_2}}\phi_{\mathrm{SiO_2}} + U^{\mathrm{Ta_2O_5}}\phi_{\mathrm{Ta_2O_5}}}{U^{\mathrm{He}}} \tag{92}$$

Here U is the energy stored in the material; ϕ is the acoustic loss angle for the material.

To find the stored energy, we use the treatment above to find the displacement field in each layer. The stored energy can then be expressed as

$$\begin{aligned} U_j^{\mathrm{stored}} &\propto \int_0^{d_j} \omega_\beta^2 \rho_j |s_j^{(\mathrm{f})} e^{ikn_j^{\mathrm{ac}}x} + s_j^{(\mathrm{b})} e^{-ikn_j^{\mathrm{ac}}x}|^2 dx \\ &= \omega_\beta^2 \rho_j \left[\left(|s_j^{(\mathrm{f})}|^2 + |s_j^{(\mathrm{b})}|^2 \right) d_j - \frac{1}{kn_j^{\mathrm{ac}}} \mathrm{Im} \left(s_j^{(\mathrm{f})*} s_j^{(\mathrm{b})} (e^{-2ikn_j^{\mathrm{ac}}d_j} - 1) \right) \right] \end{aligned} \tag{93}$$

The calculated ratios of energy stored in SiO_2 and Ta_2O_5 are shown in table 3. Both $\phi_{\mathrm{SiO_2}}$ and $\phi_{\mathrm{Ta_2O_5}}$ have been measured over a range of temperatures and for frequencies mostly much lower than 300 MHz [9, 10, 11, 12, 13, 14, 15, 16]. All of these measurements show $\phi_{\mathrm{SiO_2}}; \phi_{\mathrm{Ta_2O_5}} < 10^{-3}$. The values of the quality factor due to absorption in the DBR ($Q_{\beta,\mathrm{loss}}$), assuming $\phi_{\mathrm{SiO_2}} = \phi_{\mathrm{Ta_2O_5}} = 10^{-3}$, are shown in Table 3. For all designs $Q_{\beta,\mathrm{loss}}$ is much larger than $Q_{\beta,\mathrm{ext}}$. As a result, the acoustic quality factor should not be limited by the acoustic absorption in the DBR.

SI C Acoustic loss in the superfluid helium.

SI C.1 Intrinsic temperature dependent loss

For $T < 600$ mK the main intrinsic loss mechanism for density waves (i.e., first sound) in superfluid helium is the three phonon process [17]. It can be described by an amplitude attenuation coefficient α_{3pp}

$$\alpha_{3\mathrm{pp}}(\omega_\beta) = \frac{\pi^2 (u+1)^2 k_B^4}{30 \rho_{He} \hbar^3 v_{He}^6} \omega_\beta T^4 \left(\arctan(\omega_\beta \tau) - \arctan\left(\frac{3}{2} \gamma \bar{p}^2 \omega_\beta \tau \right) \right) \tag{94}$$

Here ω_β is the wave frequency, T is the temperature, $\rho_{He} = 145$ kg/m^3 and $v_{He} = 238$ m/s are the helium density and sound velocity, $u = 2.84$ is the Grüneisen constant [18], $\tau = \xi T^{-5}$ is the thermal phonon lifetime, where $\xi = 1.11 \times 10^{-7}$ s·K^5 [19] and $\bar{p} = 3k_B T / v_{He}$ is the average thermal phonon momentum. Finally, γ is the coefficient for the cubic term in the phonon dispersion, which is expressed as $\gamma = -\frac{1}{6v_{He}} \frac{d^3\epsilon}{dp^3}$, where ϵ and p are phonon energy and momentum respectively. It has been measured to be $\gamma = -8 \times 10^{47}$ kg^{-2}m^{-2}s^2 [18].

The intrinsic quality factor of an acoustic mode can be calculated from the attenuation length as

$$Q_{\beta,\mathrm{int}} = \frac{\omega_\beta}{2 v_{He} \alpha_{3pp}} \tag{95}$$

For the relevant acoustic mode frequency $\omega_\beta = 2\pi \times 313.86$ MHz and temperature $T < 0.5$ K both $\arctan$ arguments in equation 94 are $\gg 1$, leading to the simple relationship

$$Q_{\beta,\text{int}} = \frac{\chi}{T^4}, \tag{96}$$

where $\chi \approx 118$ K^4.

SI C.2 Heat transport model and thermal response time.

In order to make use of the equations 94 and 95 to analyze the data in the main paper, it is necessary to know the temperature of the helium inside the cavity. To accomplish this, we have developed a model of heat transport in the device. The steady state solution of this model yields the dependence of the device temperature on the dissipated power and the temperature of the mixing chamber, and is used to derive equation 2 in the main text. The dynamical solution provides an expression for the thermal relaxation time of the helium inside the cavity.

Heat transport equation

First, let us define the geometry of the device. As shown in figure 1a of the main text, a cylindrical volume of helium occupies the space between the faces of two optical fibers which are confined within the bore of a glass ferrule. The helium inside the cavity is thermally linked to a larger volume of helium outside the ferrule via two identical sheaths; since these sheaths have the same length, we can represent them as a single sheath with doubled cross-sectional area. Finally, we assume that the helium outside the ferrule has large heat capacitance and a good thermal link to the mixing chamber, so its temperature doesn't depend on the power dissipated inside the cavity and is the same as the mixing chamber temperature.

We represent the helium inside the cavity as a point heat capacitance $C_0(T)$ located at $x = l$ and experiencing a heat load Φ (dissipated laser power). This capacitance is connected to a reservoir at $x = 0$ through a one-dimensional channel (the combined sheaths), which has a heat capacitance per unit length $C_l(T)$ and a thermal resistance per unit length $R_l(T)$. The reservoir is maintained at a constant temperature T_{MC}. If we denote the temperature dependent specific heat (per unit volume) of helium by $c_V(T)$ and its thermal conductivity in the channel by $\kappa(T)$, we get for the parameters above

$$C_0(T) = V_{\text{cav}} c_V(T) \tag{97}$$

$$C_l(T) = A_{\text{sh}} c_V(T) \tag{98}$$

$$R_l(T) = (A_{\text{sh}}\kappa(T))^{-1}, \tag{99}$$

where V_{cav} is the volume of the cylindrical cavity and A_{sh} is the combined cross-sectional area of the sheaths.

The two equations governing the heat transport in the channel are

$$j = -\frac{1}{R_l(T)}\frac{\partial T}{\partial x} \tag{100}$$

$$C_l(T)\frac{\partial T}{\partial t} = -\frac{\partial j}{\partial x} \tag{101}$$

DOI: 10.1038/NPHYS3900

The first equation relates the heat current $j(x)$ and the temperature gradient $\frac{\partial T}{\partial x}$ (positive values of j denote the heat flowing in the positive x direction, i.e., from the reservoir into the cavity), and the second one describes the heating of the helium inside the channel. The boundary condition at the reservoir is simply $T(x=0) = T_{\mathrm{MC}}$, while for the cavity it is expressed through a heat flow balance

$$\Phi = \left(C_0 \frac{\partial T}{\partial t} - j \right) \Big|_{x=l} \tag{102}$$

This last relation shows that the power Φ dissipated in the cavity is partially spent on increasing its temperature and partially transmitted into the channel.

Because the thermal conductivity κ and heat capacity c are temperature-dependent, the equations above are in principle non-linear. Nevertheless, since they have the same dependence $c(T) = \delta_V T^3$, $\kappa(T) = \epsilon_V T^3$, we can transform the equations into linear ones with an appropriate substitution. For that, we express the material parameters as

$$C_l(T) = A_{\mathrm{sh}} c(T) = \delta_l T^3 \tag{103}$$
$$C_0(T) = V_{\mathrm{cav}} c(T) = \delta_0 T^3 \tag{104}$$
$$R_l(T) = (A_{\mathrm{sh}} \kappa(T))^{-1} = (\epsilon_l T^3)^{-1}, \tag{105}$$

where $\delta_l = A_{\mathrm{sh}} \delta_V$, $\delta_0 = V_{\mathrm{cav}} \delta_V$ and $\epsilon_l = A_{\mathrm{sh}} \epsilon_V$. Substituting these expressions into the equation and boundary conditions, we obtain

$$j(x) = -\epsilon_l T^3 \frac{\partial T}{\partial x} = -\frac{\epsilon_l}{4} \frac{\partial (T^4)}{\partial x} \tag{106}$$

$$-\frac{\partial j}{\partial x} = \delta_l T^3 \frac{\partial T}{\partial t} = \frac{\delta_l}{4} \frac{\partial (T^4)}{\partial t} \tag{107}$$

$$\Phi = \left(\delta_0 T^3 \frac{\partial T}{\partial t} - j \right) \Big|_{x=l} = \left(\frac{\delta_0}{4} \frac{\partial (T^4)}{\partial t} - j \right) \Big|_{x=l} \tag{108}$$

Denoting $u = T^4$ and using the first equation to express j leads to

$$\frac{\partial u}{\partial t} = \frac{\epsilon_l}{\delta_l} \frac{\partial^2 u}{\partial x^2} \tag{109}$$

$$u|_{x=0} = u_0 \tag{110}$$

$$\left(\frac{\partial u}{\partial t} + \frac{\epsilon_l}{\delta_0} \frac{\partial u}{\partial x} \right) \Big|_{x=l} = \frac{4\Phi}{\delta_0} \tag{111}$$

Thus, the heat transport equation is expressed as a one-dimensional diffusion equation with the diffusion coefficient $D = \epsilon_l / \delta_l$.

Steady state solution

First, we consider a steady state solution with a constant heat load Φ. The diffusion equation turns into $\frac{\partial^2 u}{\partial x^2} = 0$, which has a general solution $u = a + bx$. The boundary condition at $x = 0$ immediately yields $a = u_0 = T_{\rm MC}^4$. From the second boundary condition we find $b = \frac{\partial u}{\partial x} = \frac{4\Phi}{\epsilon_l}$, which results in

$$u(x) = u_0 + \frac{4\Phi}{\epsilon_l} x, \tag{112}$$

From this, the temperature of the cavity can be determined as

$$T_{\rm cav}^4 = u(l) = T_{\rm MC}^4 + \frac{4\Phi}{\epsilon_l} l \tag{113}$$

This relation is used to derive equation 2 in the main text.

Transient dynamics

Next, we consider the dynamics of this system. We consider the system in the steady state derived above and then abruptly turn off the power source at $t = 0$. The cavity temperature should then decay to T_0 exponentially with some characteristic time τ_0, which we want to determine.

To find the time evolution we use the eigenfunctions expansion of the solution:

$$u(x,t) = u_0 + \sum_n T_n(t) v_n(x), \tag{114}$$

where $v_n(x)$ is an eigenfunction of the Laplace operator with the appropriate boundary conditions

$$\frac{\partial^2 v_n}{\partial x^2} = -\lambda_n v_n \tag{115}$$

$$v_n(0) = 0 \tag{116}$$

$$\left(\frac{\epsilon_l}{\delta_l} \frac{\partial^2 v_n}{\partial x^2} + \frac{\epsilon_l}{\delta_0} \frac{\partial v_n}{\partial x} \right) \bigg|_{x=l} = 0 \tag{117}$$

If we denote $\lambda_n = k_n^2$ (choosing the opposite sign $\lambda = -k_n^2$ results in the inability to satisfy both boundary conditions simultaneously, as well as an exponentially diverging time evolution), we get from the first two equations that $v_n(x) = \sin(k_n x)$. The boundary condition at $x = l$ restricts the values of k_n

$$-\frac{\epsilon_l}{\delta_l} k_n^2 \sin(k_n l) + \frac{\epsilon_l}{\delta_0} k_n \cos(k_n l) = 0, \tag{118}$$

which can be rewritten as

$$(k_n l) \tan(k_n l) = r_V \tag{119}$$

with $r_V = \frac{l\delta_l}{\delta_0} = \frac{lA_{sh}}{V_{cav}} = \frac{V_{sh}}{V_{cav}}$ is the ratio of the sheath and the cavity volumes. The solutions for this equation exhaust all of the values k_n.

Now we can substitute the expansion back into equation 109 to obtain the equations for the time-dependent parts T_n:

$$\frac{\partial u}{\partial t} = \frac{\epsilon_l}{\delta_l} \frac{\partial^2 u}{\partial x^2} \tag{120}$$

$$\sum_n v_n \frac{\partial T_n}{\partial t} = \frac{\epsilon_l}{\delta_l} \sum_n T_n \frac{\partial^2 v_n}{\partial x^2} = -\frac{\epsilon_l}{\delta_l} \sum_n k_n^2 T_n v_n \tag{121}$$

 DOI: 10.1038/NPHYS3900

As the eigenfunctions are orthogonal, equation 121 has to be satisfied for each T_n independently

$$\frac{\partial T_n}{\partial t} = -\frac{\epsilon_l k_n^2}{\delta_l} T_n = -\frac{T_n}{\tau_n}, \tag{122}$$

where $\tau_n = \frac{\delta_l}{\epsilon_l k_n^2}$ is the characteristic decay time. The solution for this equation is

$$T_n(t) = T_n(0) e^{-t/\tau_n}, \tag{123}$$

We're mostly interested in the longest relaxation time τ_0 corresponding to the smallest value of k_n, which we denote as k_0

$$\tau_0 = \frac{\delta_l}{\epsilon_l} \frac{1}{k_0^2} \tag{124}$$

With several percent error, k_0 can be approximated by

$$(k_0 l)^{-2} \approx \left(\frac{2}{\pi}\right)^2 + r_V, \tag{125}$$

so the relaxation time becomes

$$\tau_0 \approx \frac{\epsilon_l}{\delta_l} l^2 \left(\frac{4}{\pi^2} + r_V\right) = \frac{\delta_l T^3 l}{\epsilon_l T^3 / l} \left(\frac{4}{\pi^2} + r_V\right) = \frac{c l^2}{\kappa} \left(\frac{4}{\pi^2} + r_V\right) = \frac{C_{\mathrm{sh}}}{K_{\mathrm{sh}}} \left(\frac{4}{\pi^2} + r_V\right), \tag{126}$$

where $C_{\mathrm{sh}} = c A_{\mathrm{sh}} l = \delta_l T^3 l$ is the total heat capacitance of the sheath, and $K_{\mathrm{sh}} = \kappa A_{\mathrm{sh}}/l = \epsilon_l T^3 / l$ is the total thermal conductance of the sheath.

The expression above for the thermal relaxation time τ_0 depends only the sheath's heat capacitance, thermal conductance, and the geometric parameter r_V. The heat capacitance of the sheath can be known fairly well, since it only depends on its volume and the specific heat of the liquid helium, which for low temperatures is well known [20]. Thermal conductivity, however, is much harder to evaluate *a priori*, since it depends upon the particular geometry of the conducting channel (which determines the mean phonon travel length between collisions with the boundaries) and the scattering properties of its wall. Therefore, measurements of τ_0 can provide an estimate for the thermal conductivity without the need for any assumptions about the specularity of reflections from sheath surface.

Measurement of the thermal relaxation time

We measure τ_0 by changing the circulating optical power (which is proportional to the power dissipated inside the cavity) and monitoring the response of the temperature-dependent linewidth of the acoustic mode. The experiment is performed using the OMIT/OMIA technique described in the main text, but with the probe beam frequency ω_{probe} being fixed exactly one acoustic frequency away from the control beam: $\omega_{\mathrm{probe}} = \omega_{\mathrm{control}} + \omega_\beta$. This way, the magnitude of the OMIA part of the probe beam reflection is inversely proportional to the linewidth of the acoustic mode, which is a monotonic function of the device temperature. Hence, by observing the OMIA response as a function of time we can access the temperature dynamics. In practice, rather than measuring a step response to a change in the dissipated

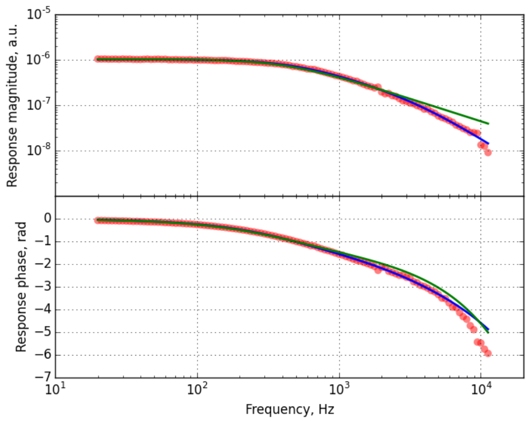

Figure 3: Amplitude and phase of the intrinsic linewidth response as a function of the modulation frequency of the circulating optical power. The blue line is the fit to a double exponential (127); for comparison, the green line shows the fit to a simple exponential decay with a time delay, which corresponds to setting $\tau_1 = 0$ in the equation 127.

optical power, we perform a lock-in measurement where we sinusoidally modulate the optical drive and record the complex response of the magnitude of the OMIA signal.

The results are shown in figure 3. The data was fit to a double exponential decay with two time scales τ_s and τ_f and an additional time delay τ_d

$$\delta\gamma_{int}[\omega] \propto \frac{1}{1+i\omega\tau_s}\frac{1}{1+i\omega\tau_f}e^{i\omega\tau_d} \tag{127}$$

We attribute the longer of the two decay times $\tau_s \approx 350\ \mu$s to the thermal response. The shorter time $\tau_f \approx 40\ \mu$s is only required to account for the data at frequencies above 2 kHz; it might arise from some other faster thermal process in the system (e.g., heating of the dielectric stack, or thermal equilibration of the helium inside the cavity), or from the time-delayed mechanical response itself. Finally, the time delay $\tau_d \approx 30\ \mu$s can be attributed to the sound propagation delay, as it is comparable to the ballistic phonon travel time in the sheath $l/v_{He} \approx 12\ \mu$s. In interpreting the slowest time τ_s as the thermal response time τ_0 we assumed that the thermal response is the slowest time scale in the system. Indeed, the slower time τ_s we observe is much larger than either optical ($\kappa_\alpha^{-1} \lesssim 3$ ns) or mechanical ($\gamma_\beta^{-1} \lesssim 20\ \mu$s) lifetime, and we are not aware of any other similarly slow process occurring inside the device.

Finally, we use the measured value of τ_0 to estimate the thermal conductance. First, we need to calculate the heat capacity, for which we can use the known value for the specific heat $c_\nu/T^3 = 8.3 \times 10^{-2}\ \mathrm{J/(mol \cdot K^4)}$ [20], which leads to the heat capacity per unit volume $c_V/T^3 = 3 \times 10^3\ \mathrm{J/(K^4 \cdot m^3)}$. Next, we evaluate the volumes. The cavity has a diameter of $d_{\mathrm{cav}} = 133 \pm 5\ \mu$m and the length of $l_{\mathrm{cav}} = 70\mu$m, so its volume is $V_{\mathrm{cav}} = \frac{\pi}{4} d_{\mathrm{cav}}^2 l_{\mathrm{cav}} = (1.0 \pm 0.1) \times 10^{-12}\ \mathrm{m}^3$. The sheaths have the same outer diameter d_{cav} (which is set by the inner diameter of the ferrule), the inner diameter d_{sh}=125 μm and the length of $l = 3$ mm; this means that the combined volume of two sheaths $V_{\mathrm{sh}} = A_{\mathrm{sh}} l = 2\frac{\pi}{4}(d_{\mathrm{cav}}^2 - d_{\mathrm{sh}}^2) l = (3.5 \div 16) \times 10^{-12}\ \mathrm{m}^3$. The large spread in the volume estimates is due to the uncertainty in the sheath thickness $h_{sh} = (d_{\mathrm{sh}} - d_{\mathrm{cav}})/2 = (1.5 \div 6.5)\ \mu$m. From the volume estimates

DOI: 10.1038/NPHYS3900

we obtain $r_V = 0.06 \div 0.27$ and $C_{\text{sh}}/T^3 = (1.0 \div 4.8) \times 10^{-8}$ J/K^4. Using the experimental value for the time constant $\tau_0 = 3.5 \times 10^{-4}$ s we get $K_{\text{sh}}/T^3 \equiv \epsilon = (2.5 \div 7.8) \times 10^{-5}$ W/K^4.

We can assess the validity of this result using the theoretical expression for the thermal conductivity of a cylindrical channel[21]:

$$\kappa(T) = \frac{1}{3} c(T) v_{He} d_{\text{ch}} \frac{2-f}{f}, \tag{128}$$

which is applicable when the phonon mean free path is limited by the scattering at the channel boundaries. Here d_{ch} is the diameter of the channel, and f is the fraction of diffusive phonon scattering events at the channel walls. This equation can be rewritten as

$$\frac{2-f}{f} = \frac{3}{v_{He} d_{\text{ch}}} \frac{\kappa(T)}{c(T)} \tag{129}$$

We can apply this formula to the sheath by using equation 126 to express the ratio c/κ. With that, we find

$$\frac{2-f}{f} = \frac{3}{v_{He} d_{\text{ch}}} \frac{l^2}{\tau_0} \left(\frac{4}{\pi^2} + r_V \right) \tag{130}$$

If we approximate d_{ch} by twice the sheath thickness (to account for the much longer longitudinal scattering events) $d_{\text{ch}} \approx 2h_{sh} = d_{\text{cav}} - d_{\text{sh}} = (3 \div 13)$ μm, we will find that the diffusive scattering fraction f is between 3% for the minimal sheath thickness of 1.5 μm and 20% for the maximal sheath thickness of 6.5 μm. These values appear reasonable for the optically smooth glass surfaces of the ferrule and the fiber and typical wavelength of thermal phonons $\lambda_{\text{th}} = 2\pi \frac{\hbar v_{He}}{3k_B T} \gtrsim 10$ nm for $T < 0.4$ K.

SI D Cooperativity

In this section, we describe how the optomechanical cooperativity C and the single-photon cooperativity C_0 are influenced by the cavity geometry and thermal conductance. Optomechanical cooperativity is defined in [22] as:

$$C = \frac{4(g^{\alpha,\beta})^2}{\kappa_\alpha \gamma_\beta} = \frac{4(g_0^{\alpha,\beta})^2 \bar{n}_\alpha}{\kappa_\alpha \gamma_\beta} = \bar{n}_\alpha C_0 \tag{131}$$

It is an important figure of merit in optomechanics, quantifying the efficiency of the system in exchanging photons and phonons [22]. Large cooperativity is necessary, e.g. for squeezing of light ($C > n_{\text{th}}(1+(2\omega_m/\kappa)^2)$) [23], efficient state transfer between optical and mechanical modes ($C > n_{\text{th}}$) [24], and cooling the mechanical oscillator ($n = \frac{n_{\text{th}} + C(\kappa/4\omega_m)^2}{C+1}$) , where n is the lowest achievable phonon number [22]. While C is of interest, it is partially determined by the maximum number of photons that can be stored within the cavity. Since this number is typically limited by thermal constraints or optical nonlinearities, it is also useful to quantify device performance by defining the power-independent quantity C_0 (single photon cooperativity) .

SI D.1 Single photon cooperativity

Here we describe how the single photon cooperativity C_0 depends on the cavity geometry. As shown in equation 131, it depends on $g_0^{\alpha,\beta}$, κ_α and γ_β, all of which, in the case of helium confined in a Fabry-Perot cavity and neglecting any contributions to γ_β from the helium's internal loss, are approximately inversely proportional to cavity length. Therefore we do not expect single photon cooperativity to have a strong dependence on cavity length.

In this situation, for a cavity of length L, the optical linewidth κ_α and mechanical linewidth γ_β are given by [25]:

$$\kappa_\alpha = \frac{c(1 - r_1^{(\mathrm{opt})} r_2^{(\mathrm{opt})})}{L r_1^{(\mathrm{opt})} r_2^{(\mathrm{opt})}} \tag{132}$$

and

$$\gamma_\beta = \frac{v_{\mathrm{He}}(1 - r_1^{(\mathrm{ac})} r_2^{(\mathrm{ac})})}{L r_1^{(\mathrm{ac})} r_2^{(\mathrm{ac})}} \tag{133}$$

The expression for the optomechanical coupling $g_0^{\alpha,\beta}$ is given in the main text. It depends on the mode shape and size, which in turn depend on L, R_1, and R_2 (the radii of curvature of the two mirrors). As described in the main text, we use the paraxial approximation to obtain the profiles of both the acoustic and optical modes [25], and then find $g_0^{\alpha,\beta}$ by numerical integration of Eq.1 in the main text. We find that $g_0^{\alpha,\beta}$ is maximized for $R_1, R_2 \simeq 0.54L$. Intuitively this can be understood as follows. A cavity with $R_1, R_2 = 0.5L$ (i.e. a spherical configuration) is unstable with a vanishing waist and diverging spot size at the mirrors. As R_1 and R_2 increase, the waist increases, while the mode diameter at the mirror surface decreases very rapidly. If R_1 and R_2 increase too much (i.e so as to approach a plane-plane configuration), the mode's transverse dimensions again diverge. The value $R_1, R_2 \simeq 0.54L$ represents the optimal choice between these extremes.

In the specific device described here, the values of the electric field reflectivities of the mirrors for 1550 nm light provided by the manufacturer are $r_1^{(\mathrm{opt})} = 0.99995$ and $r_2^{(\mathrm{opt})} = 0.999994$ [26], consistent with the calculations in section SI B and with the maximum measured finesse. The values $r_1^{(\mathrm{ac})} = 0.995$ and $r_2^{(\mathrm{ac})} = 0.996$ are the mirrors' amplitude reflectivities for the 315.7 MHz acoustic wave as calculated in section SI B, and confirmed by the measurements of the acoustic quality factor.

We first use equations 131, 132, 133 as well as the expression for $g_0^{\alpha,\beta}$ to calculate C_0 for cavities of various L and for $R_1, R_2 = 0.54L$ assuming the mirrors are much larger than mode's transverse size (this assumption will be relaxed in what follows). For $L > 5$ μm, $C_0 \simeq 1.09 \times 10^{-3}$ and varies by less than 0.1%, so is practically independent of cavity length, confirming the qualitative reasoning above. The value C_0 is plotted in figure 4 for varying cavity lengths.

The cavity used in this experiment does not have $R_1 = R_2 = 0.54L$, but rather has $R_1 = 408$ μm, $R_2 = 292$ μm and $L = 85.2$ μm. These values were chosen as a compromise between satisfying the ideal relationship ($R_1 = R_2 = 0.54L$), minimizing the potential impact of mirror misalignment, operating in the resolved sideband regime, maintaining a transverse mode smaller than the mirrors, and accomodating the range of R that can be achieved using the laser machining technique. C_0 for such a cavity, calculated as before, and again neglecting the effect of the mirrors' finite size, is shown as a function of L in figure 5 using red squares.

 DOI: 10.1038/NPHYS3900

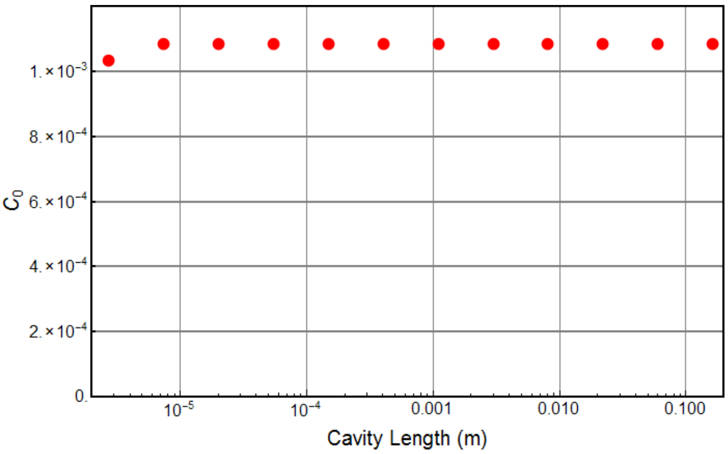

Figure 4: Single photon cooperativity for different cavity lengths L, assuming mirrors with $R_1, R_2 = 0.54L$

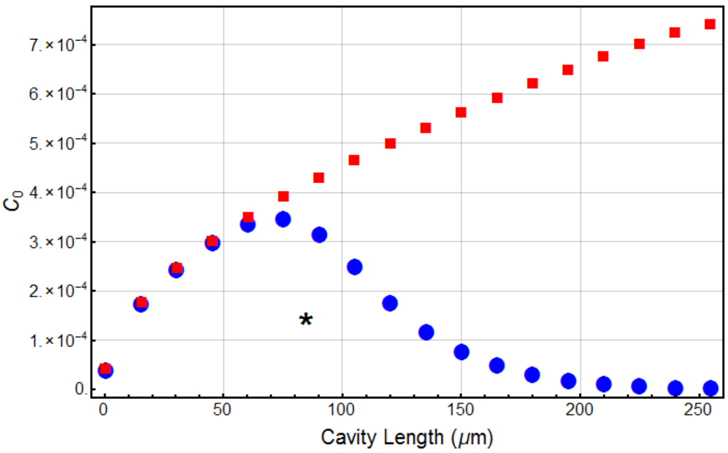

Figure 5: Single photon cooperativity for different cavity lengths for the mirrors used in the experiment.

However due to the fabrication process, the mirrors are not ideally shaped, but instead have a Gaussian profile with FWHM (Full Width at Half Maximum): $d_1 = 36$ μm, $d_2 = 41$ μm. Only inside this FWHM does the mirror efficiently confine the cavity mode; this leads to clipping losses for longer cavities [1], diminishing the optical finesse. When the contributions of these clipping losses are included in κ_α (using the treatment in [1]), the resulting C_0 is shown with blue circles in figure 5.

The single photon cooperativity extracted from the experiment via direct measurement of κ_α, γ_β and the estimate of $g_0^{\alpha,\beta}$ described in the main text is $C_0 = 1.5 \times 10^{-4}$ and is marked with a black star in figure 5. The difference from the expected value of cooperativity (blue circles) is primarily due to the fact that optical finesse achieved in the device ($\mathcal{F} = 2.56 \times 10^4$) differs from the optical finesse at this L extracted from the values of $r_1^{(\mathrm{opt})}$, $r_2^{(\mathrm{opt})}$, d_1 and d_2 ($\mathcal{F} = 4.47 \times 10^4$), which could be a result of imperfect alignment, mirror surface contamination or deviations of the mirror shape.

SI D.2 Heating limit for the optomechanical cooperativity.

As discussed in section SI C.1, heating of the helium inside the cavity causes an increase in the damping of the mechanical mode. This sets a practical limit on the incident optical power and, consequently, on the maximum multiphoton optomechanical cooperativity.

For a given heat load Φ in steady state the temperature of the cavity is given by equation 113:

$$T_{\text{cav}}^4 = T_{\text{MC}}^4 + \frac{4\Phi}{\epsilon_l} l = T_{\text{MC}}^4 + \frac{4\Phi}{\epsilon}, \tag{134}$$

where $\epsilon = \epsilon_l / l = \frac{K_{sh}}{T^3}$ is the coefficient for the temperature-dependent thermal conductance. This results in an internal damping rate (see equations 94-96)

$$\gamma_{\beta,\text{int}} = \frac{\omega_\beta}{Q_{\beta,\text{int}}} = \frac{\omega_\beta}{\chi} T_{\text{cav}}^4 = \frac{\omega_\beta}{\chi}\left(T_{\text{MC}}^4 + \frac{4\Phi}{\epsilon}\right) \tag{135}$$

The total damping is the of this intrinsic damping and the acoustic radiation set by the acoustic transmission at the helium-glass interface:

$$\gamma_\beta = \gamma_{\beta,\text{int}} + \gamma_{\beta,\text{rad}} = \frac{4\omega_\beta}{\chi\epsilon}\Phi + \frac{4\omega_\beta}{\chi} T_{\text{MC}}^4 + \gamma_{\beta,\text{rad}} \tag{136}$$

Thus, γ_β has three main components:

(i) The intrinsic loss due to the optical heating

$$\gamma_{\beta,\Phi} = \frac{4\omega_\beta}{\chi\epsilon}\Phi \tag{137}$$

As noted in the main text, we can relate the heat load Φ to the incident power P_{inc} and the circulating photon number $\bar{n}_\alpha$:

$$\Phi = \mu P_{\text{inc}} + \nu\hbar\omega_\alpha\kappa_{\alpha,\text{int}}\bar{n}_\alpha \tag{138}$$

This allows us to express the mechanical damping as

$$\gamma_{\beta,\Phi} = a_{\text{inc}} P_{\text{inc}} + a_{\text{circ}}\bar{n}_\alpha \tag{139}$$

with the coefficients $a_{\text{inc}} = 4\mu\omega_\beta/(\chi\epsilon)$ and $a_{\text{circ}} = (4\nu\hbar\omega_\alpha\kappa_{\alpha,\text{int}}\omega_\beta)/(\chi\epsilon)$. Using the experimentally determined values of μ/ϵ and ν/ϵ (provided in the main text) we find these to be $a_{\text{inc}} = 2\pi \cdot (1.3 \pm 0.2) \cdot 10^8$ Hz/W and $a_{\text{circ}} = 2\pi \cdot (2.1 \pm 0.2)$ Hz.

Both of these coefficients are inversely proportional to the thermal conductance coefficient ϵ, meaning that improving the device thermalization enhances its power handling. In the present device the cavity is thermalized through a relatively long and narrow sheath of helium, as described in the main text, it should be possible to achieve a significant increase in thermal conductance by a small change the device construction. We can estimate this increase by using a standard result from kinetic theory, which is a generalization of equation 128:

$$\kappa = \frac{1}{3} c v_{He} \lambda, \tag{140}$$

 DOI: 10.1038/NPHYS3900

where λ is the phonon mean free path. The corresponding thermal conductance for a 1D channel of cross-sectional area A and length l is

$$K = \frac{\kappa A}{l} = \frac{1}{3}\frac{c v_{He} \lambda A}{l} \tag{141}$$

For estimate we can assume a geometry where the cavity is formed between the two fiber faces as in the current device, but is not confined inside the alignment ferrule (e.g., each fiber is held in a separate ferrule with $\sim 500\ \mu\mathrm{m}$ gap between the ferrule faces, as in [27]). For $\sim 60\ \mu$m long cavity and $\sim 125\ \mu$m fiber diameter we can approximate all relevant dimensions (including the mean free path) as 100 μm: $l \approx \lambda \approx 100\ \mu$m, $A \approx (100\ \mu\mathrm{m})^2$. This results in the heat conductance $K/T^3 = 2 \cdot 10^{-3}\ \mathrm{W/K^4}$, which is to be compared to the sheath conductance $K_{\mathrm{sh}}/T^3 = (2.5 \div 7.8) \times 10^{-5}\ \mathrm{W/K^4}$. Thus, it seems feasible to increase the heat conductance by a factor of 30. Assuming that the fraction of the optical losses dissipating into heat stays the same, we find that for such a device $a_{\mathrm{inc}} \approx 2\pi \cdot 4 \cdot 10^7$ Hz/W and $a_{\mathrm{circ}} = 2\pi \cdot 7 \cdot 10^{-2}$ Hz.

(ii) The second loss source is the intrinsic damping due to the finite mixing chamber temperature

$$\gamma_{\beta,\mathrm{MC}} = \frac{4\omega_\beta}{\chi} T_{\mathrm{MC}}^4 \tag{142}$$

In the experiment the lowest achieved mixing chamber temperature is about 10 mK, and it consistently stayed below 50 mK unless a heater was used. This puts the associated damping below 20 Hz (corresponding to the quality factor $> 1.5 \cdot 10^7$), which can be neglected compared to the effects of the cavity thermalization discussed in the previous paragraph.

(iii) The last is the radiative loss associated with sound transmission through the helium/glass interface. This is described in detail in chapter SI B. Here we just note that this damping is independent of temperature, and that in the current device it limits the quality factor to 79,000 $\pm$ 5,000 ($\gamma_{\beta,\mathrm{rad}} = 2\pi \cdot (4.0 \pm 0.3)$ kHz); implementing an acoustic DBR (described in section SI B.5) can raise the quality factor to $(3.3 \pm 2.2) \cdot 10^6$ ($\gamma_{\beta,\mathrm{rad}} = 2\pi \cdot 100$ Hz).

Expressions 131, 136 and 139 can be used to calculate the dependence of the multiphoton cooperativity on the incident optical power. In determining the circulating photon number we assume that 10% of the incident power is in the control beam detuned by ω_β away from the cavity resonance, while the rest is in the optical local oscillator (OLO) detuned by about 1 GHz.

The results are shown in the left panel of figure 6. All of the lines demonstrate the same trend: for low powers the mechanical damping is dominated by the radiative losses and is independent of the incident power, so the cooperativity grows linearly with P_{inc}; for high powers the mechanical linewidth is proportional to the incident power, and the cooperativity levels out. The theoretical calculations for the present device are denoted by a solid red line, with the black star denoting the maximal cooperativity obtained during Brownian motion measurements. The dashed red line corresponds to an increased radiative quality factor $Q_{\mathrm{rad}} = 3.3 \cdot 10^6$ (achieved by adding acoustic DBR, as discussed in section SI B.5), which improves the cooperativity at low power, but doesn't affect the saturation value. The solid blue line is the same as solid red, but it assumes a $30\times$ increase in the thermal conductivity; this improves the high power behavior and maximal achievable cooperativity, but leaves the low power dependence the same. The dashed blue line includes both of these improvements, leading to a $\sim$30-fold increase

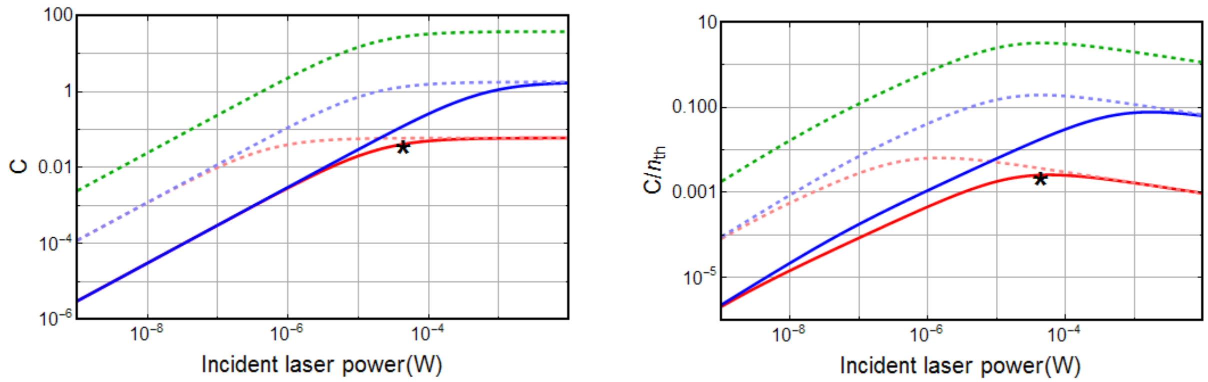

Figure 6: Dependence of the multiphoton cooperativity C (left) and thermal multiphoton cooperativity C/n_{th} (right) on incident laser power. Line style denotes radiative mechanical losses $\gamma_{\beta,\mathrm{rad}}$: solid lines correspond to $Q_{\beta,\mathrm{rad}} = 70,000$ (as for the current device), while dashed lines represent a device with $Q_{\beta,\mathrm{rad}} = 3.3 \cdot 10^6$. The line color denotes the intrinsic temperature dependent mechanical damping $\gamma_{\beta,\Phi}$: red lines describe the current device, while the blue and the green lines suppose a factor of 30 improvement in thermal conductance. All the lines except for the green assume that 10% of the incident power is in the control beam detuned by 320 MHz from the cavity resonance; for the green line 100% of the incident power is in the control beam. In addition, the green line assumes that the optical linewidth is decreased from 69 MHz to 30 MHz (while keeping cavity length the same) and that the relative input coupling $\kappa_{\alpha,\mathrm{in}}/\kappa_\alpha$ is increased from 0.25 to 0.5. The black star denotes the maximum $C \simeq 0.041$ and $C/n_{\mathrm{th}} \simeq 0.0025$ measured in the device. In those measurements the incident power was 46 μW, mixing chamber temperature was 60 mK, total circulating photon number was $\simeq 2000$ of which $\simeq 1000$ photons were coming from the control beam. The control beam had $\simeq 9$ % of the total incident power.

of cooperativity for all powers. Finally, the dashed green lines assumes additionally a decrease in the optical linewidth from 69 MHz to 30 MHz, an increase of the relative input coupling from 0.25 to 0.5, and the absence of the OLO, so that all of the incident power is concentrated in the control beam (which decreases the contribution to the thermal load associated with the OLO).

The right part of figure 6 shows another figure of merit, the thermal cooperativity, which is defined as a ratio of the multiphoton cooperativity to the equilibrium thermal phonon occupation. This quantity is important for quantifying the efficiency of quantum protocols, as it represents the ratio of the measurement strength to the thermal decoherence rate of the mechanical oscillator. In determining the phonon occupation, the equilibrium temperature of the mechanical oscillator is assumed to be equal to the helium temperature inside the cavity T_{cav} calculated using expression 113, which is consistent with the data from figure 4(c) in the main paper. For the optimized device (dashed green line) the thermal cooperativity exceeds unity for a wide range of powers, and can become as large as 5.

References

[1] D. Hunger et al. A fiber Fabry Perot cavity with high finesse. *New J. Phys.*, 12(6):065038, 2010.

DOI: 10.1038/NPHYS3900

[2] L. R. Brovelli and U. Keller. Simple analytical expressions for the reflectivity and the penetration depth of a Bragg mirror between arbitrary media. *Opt. Commun.*, 116(4-6):343–350, 1995.

[3] I. Koné et al. Guided acoustic wave resonators using an acoustic Bragg mirror. *Appl. Phys. Lett.*, 96(22):223504, 2010.

[4] A. Soukiassian et al. Acoustic Bragg mirrors and cavities made using piezoelectric oxides. *Appl. Phys. Lett.*, 90(4):042909, 2007.

[5] R. J. Donnelly and C. F. Barenghi. The observed properties of liquid helium at the saturated vapour pressure. *J. Phys. Chem. Ref. Data*, 27(6), 1998.

[6] Correspondence with LaserOptik mirror coating company, 2014.

[7] J. Capilla et al. Characterization of amorphous tantalum oxide for insulating acoustic mirrors. *2011 Jt. Conf. IEEE Int. Freq. Control Eur. Freq. Time Forum Proc.*, pages 1–6, 2011.

[8] J. T. Krause. Anomalous temperature-frequency dependence of acoustic properties of vitreous silica at low temperatures. *Phys. Lett. A*, 43(4):325–326, 1973.

[9] S. D. Penn et al. Mechanical loss in tantala/silica dielectric mirror coatings. *Class. Quantum Gravity*, 20(13):2917–2928, 2003.

[10] D. R. M. Crooks et al. Experimental measurements of mechanical dissipation associated with dielectric coatings formed using SiO_2, Ta_2O_5 and Al_2O_3. *Class. Quantum Gravity*, 23(15):4953–4965, 2006.

[11] K. Numata et al. Systematic measurement of the intrinsic losses in various kinds of bulk fused silica. *Phys. Lett. Sect. A Gen. At. Solid State Phys.*, 327:263–271, 2004.

[12] I. Martin et al. Comparison of the temperature dependence of the mechanical dissipation in thin films of Ta_2O_5 and Ta_2O_5 doped with TiO_2. *Class. Quantum Gravity*, 26(15):155012, 2009.

[13] E. Hirose et al. Mechanical loss of a multilayer tantala/silica coating on a sapphire disk at cryogenic temperatures: Toward the KAGRA gravitational wave detector. *Phys. Rev. D*, 90:2–7, 2014.

[14] K. Yamamoto and S. Miyoki. Mechanical Loss of Reflective Coating at Low Temperature. In *Int. Cosm. Ray Conf.*, pages 3111–3114, 2003.

[15] M. Principe et al. Material loss angles from direct measurements of broadband thermal noise. *Phys. Rev. D*, 91:1–10, 2015.

[16] R. O. Pohl, X. Liu, and E. Thompson. Low-temperature thermal conductivity and acoustic attenuation in amorphous solids. *Rev. Mod. Phys.*, 74(October):991–1013, 2002.

[17] H. J. Maris and W. E. Massey. Phonon Dispersion and the Propagation of Sound in Liquid Helium-4 below 0.6° K. *Phys. Rev. Lett.*, 25(4):25–27, 1970.

[18] H. J. Maris. Attenuation and velocity of sound in superfluid helium. *Phys. Rev. Lett.*, 28(5):277–280, 1972.

[19] J. Jäckle and K. W. Kehr. Note on phonon lifetimes in He II. *Phys. Lett. A*, 37(3):205–206, 1971.

[20] F. Pobell and J. Brooks. *Matter and Methods at Low Temperatures*, volume 45. 1992.

[21] B. Bertman and T.A. Kitchens. Heat transport in superfluid filled capillaries. *Cryogenics (Guildf).*, 8(1):36–41, 1968.

[22] M. Aspelmeyer, T. J. Kippenberg, and F. Marquardt. Cavity optomechanics. *Rev. Mod. Phys.*, 86(December), 2014.

[23] T. P. Purdy, P. L. Yu, R. W. Peterson, N. S. Kampel, and C. A. Regal. Strong Optomechanical Squeezing of Light. *Phys. Rev. X*, 3(3):031012, sep 2013.

[24] T. A. Palomaki, J. W. Harlow, J. D. Teufel, R. W. Simmonds, and K. W. Lehnert. Coherent state transfer between itinerant microwave fields and a mechanical oscillator. *Nature*, 495(7440):210–214, 2013.

[25] A. E. Siegman. *Lasers*. 1986.

[26] Correspondence with Advanced Thin Films mirror coating company, 2014.

[27] N. E. Flowers-Jacobs et al. Fiber-cavity-based optomechanical device. *Appl. Phys. Lett.*, 101(22):221109, 2012.